ROYAL SOCIETY
OF CHEMISTRY

PAPER

Check for updates

Synergetic effect of dual co-catalysts on the activity of BiVO₄ for photocatalytic carbamazepine degradation†

Beibei Wang,[a] Ping Li,[b] Chunlei Du,[b] Yan Wang,[b] Daxin Gao,[b] Songtao Li,[b] Liying Zhang[b] and Fuyu Wen [iD] *[b]

An efficient visible-light driven three components photocatalyst for carbamazepine (CBZ) degradation has been assembled by co-loading reduction cocatalyst Pt and oxidation cocatalyst Co_3O_4 (MnO_x) on $BiVO_4$. The apparent rate constant of the three components photocatalyst $Pt/BiVO_4/Co_3O_4$ for degradation of CBZ is 54 times that of $Co_3O_4/BiVO_4$ and 2.5 times that of $Pt/BiVO_4$, which shows a synergetic effect in the photocatalytic activity. The same synergetic effect is also observed for $Pt/BiVO_4/MnO_x$. The spatial separation of the reduction and oxidation cocatalysts could reduce the recombination of the photogenerated charges, which mainly accounts for the high photocatalytic activity of the three components photocatalyst. The photocatalytic intermediates of CBZ were detected by HPLC-ESI-MS, and a deductive degradation pathway of CBZ was proposed.

1. Introduction

Pharmaceuticals and personal care products (PPCPs) are persistent organic pollutants which cannot be completely removed by conventional treatment plants.[1] For instance, the removal efficiency of carbamazepine (CBZ) through wastewater treatment plants (WWTPs) is mostly below 10%.[2] Drug residues in the natural environment eventually affect water quality, ecosystems and human health.[3] For example CBZ is reported to be toxic even at concentrations below 100 mg L^{-1}.[4] Therefore, it is urgent to seek more efficient technologies for the degradation of CBZ-containing waste-water.

Heterogeneous photocatalysis is one of the most ideal techniques because of its advantages of lower energy consumption, no secondary pollution, easy accessibility and so on.[5] To date, the most widely employed semiconductor for CBZ degradation is TiO_2,[6–9] however, it is severely limited as a sunlight-driven photocatalyst due to large band gap and low quantum yield.[10,11] Therefore substantial research efforts have aimed to develop more efficient visible-light driven photocatalyst for CBZ degradation.[12–16]

Many semiconductors possess suitable band gap (*e.g.* 2.31 eV for $BiVO_4$ which corresponding an absorption edge at 535 nm) and sufficient band potentials for CBZ degradation but without or with low activity. The recombination of the photogenerated

electrons and holes may be the main reason. To enhance the separation efficiency of the photogenerated charges, cocatalysts which serve as the active sites for the photocatalytic reactions are usually necessary.[17–24] Moreover, when both the reduction and oxidation cocatalysts were co-loaded on the semi-conductors, the synergistic effect on the photocatalytic activities were usually achieved.[25–29] The strategy of dual cocatalysts has been successfully employed in photocatalytic water split-ting,[26,27,29,30] photocatalytic oxidation of some pollutants such as thiophene[28,31] and some dyes.[25,26,28] However, the synergistic effect of dual cocatalysts is far less investigated in the photo-catalytic degradation of pharmaceuticals.

Herein we report an efficient visible-light driven three components photocatalyst for carbamazepine degradation. By co-loading reduction cocatalyst Pt and oxidation cocatalyst Co_3O_4 (MnO_x) on $BiVO_4$, the three components photocatalysts $Pt/BiVO_4/Co_3O_4$ (MnO_x) were assembled. The apparent rate constant of $Pt/BiVO_4/Co_3O_4$ for degradation of carbamazepine is 54 times of $Co_3O_4/BiVO_4$ and 2.5 times of $Pt/BiVO_4$, which shows a synergetic effect in the photocatalytic activity. The present work further demonstrates the universality of the strategy of dual-cocatalysts, which would be useful to construct highly efficient photocatalyst for pharmaceuticals degradation.

2. Experimental

2.1 Catalyst preparation

All of the reagents were of analytical grade, and were used without further purification. $BiVO_4$ was prepared by a hydro-thermal process.[31] The precursors NH_4VO_3 (12 mmol) and

[a]*Educational Technology Center, Chengde Medical University, Chengde 067000, China*
[b]*Hebei Key Laboratory of Research and Development for Traditional Chinese Medicine, Chengde Medical University, Chengde 067000, China. E-mail: wenfuyu@vip.163.com*
† Electronic supplementary information (ESI) available. See DOI: 10.1039/c9ra07152k

$Bi(NO_3)_3 \cdot 5H_2O$ (12 mmol) were dissolved in 45 mL and 15 mL of 2.0 M nitric acid solutions, respectively. Then the above solutions were mixed to form a yellow homogeneous solution. The pH value of the solution was then adjusted to 2.0 with ammonia solution under stirring. The orange mixture was stirred for 0.5 h and aged for an additional 2 h. The orange precipitate at the bottom of the beaker was transferred to a 100 mL Teflon-lined stainless steel autoclave (70% capacity) and hydrothermal treated at 200 °C for 24 h. After the autoclave was cooled to room temperature, a vivid yellow powder was separated by filtration, washed with deionized water for more than 3 times, and then dried at 60 °C for overnight.

Co_3O_4 $(MnO_x)/BiVO_4$ was prepared by photo-deposition method.[26] $Co(NO_3)_2$ solutions (0.5 g L^{-1}) or $MnSO_4$ solutions (0.5 g L^{-1}) was used as the precursor and $NaIO_3$ was employed as the electron acceptor. Typically, 0.5 g $BiVO_4$ powder was suspended in 100 mL $NaIO_3$ solutions (0.01 M), then 1.0 mL $Co(NO_3)_2$ solution or $MnSO_4$ solution was added and the suspension was then irradiated by a 300 W Xe lamp ($\lambda > 420$ nm) under continuous stirring. After 5 h photo-deposition, the suspension was filtered, washed with deionized water for more than 3 times, and finally dried at 60 °C for overnight. The preparation of $Pt/BiVO_4$ was similar to Co_3O_4 $(MnO_x)/BiVO_4$ but using H_2PtCl_6 solution (0.374 g L^{-1}) as the precursor and water as the hole scavenger.

$Pt/BiVO_4/Co_3O_4$ (MnO_x) was prepared by simultaneous photo-deposition method.[27] 0.5 g $BiVO_4$ powder was suspended in 100 mL deionized water, then 6.0 mL H_2PtCl_6 solution and 1.0 mL $Co(NO_3)_2$ solution ($MnSO_4$ solution) were added. After 5 h photo-deposition, the suspension was filtered, washed and finally dried at 60 °C for overnight.

The electrodes of $BiVO_4$, $Pt/BiVO_4/Co_3O_4$ and $Pt/BiVO_4/MnO_x$ were prepared by electrophoretic deposition of corresponding powder on FTO substrate (1 × 2 cm²),[32] followed by drying in air and calcination at 573 K for 1 h.

2.2. Catalyst characterization

The prepared samples were characterized by X-ray powder diffraction (XRD) on a Rigaku D/Max-2500/PC powder diffractometer. Each sample powder was scanned using Cu Kα radiation with an operating voltage of 40 kV and an operating current of 200 mA. The scan rate of 5° min^{-1} was applied to record the patterns in the range of 8–80° at a step of 0.02°. Brunauer–Emmett–Teller (BET) specific surface areas of the samples were determined by nitrogen adsorption at 77 K on Micromeritics ASAP 2420 system.

UV-Vis diffuse reflectance spectra (UV-Vis DRS) were recorded on a TU-1950 UV-Vis spectrophotometer (Beijing Purkinje General Instrument Co., Ltd.) equipped with an integrating sphere. The morphologies and particle sizes were examined by a Quanta 200 FEG scanning electron microscope (SEM). X-ray photoelectron spectroscopy (XPS) measurements, using a VG ESCALAB MK2 spectrometer with monochromatized Al-Kα excitation.

Electron spin resonance (ESR) signals of radicals trapped by DMPO were recorded at ambient temperature on a Brucker

ESR A200 spectrometer. The samples were introduced into the home-made quartz cup inside the microwave cavity and illuminated with a 300 W Xe lamp (CERAMAX LX-300). The settings for the ESR spectrometer were as follows: sweep width, 140 G; microwave frequency, 9.82 GHz; modulation amplitude, 1 G.

Photoelectrochemical performances of the photoanodes were measured in a three-electrode setup, where Pt electrode and saturated mercury electrode were employed as counter and reference electrode, respectively. Electrolyte was 0.5 M Na_2SO_4 solution. A shutter was used to record both the dark and photocurrent during a single scan. A 300 W Xe lamp (Ushio-CERAMAX LX-300) and optical cutoff filter (kenko, L-42; $\lambda > 420$ nm) was used as light source. Electrochemical impedance spectroscopy (EIS) were performed on a Ivium electrochemical workstation by applying an AC voltage of 10 mV amplitude in the frequency range of 10^5 Hz to 10^{-1} Hz in 0.5 M Na_2SO_4.

2.3. Photocatalytic reaction

The photocatalytic degradation of carbamazepine (CBZ) was carried out using a 300 W Xe lamp and optical cut-off filter ($\lambda > 420$ nm). Normally, 100 mg photocatalyst was dispersed in 100 mL 10 mg L^{-1} CBZ solutions. Prior to irradiation, the suspensions were magnetically stirred in dark for 30 min to establish adsorption/desorption equilibrium between CBZ and the photocatalysts. Top irradiation was used and after different irradiation time, 3 mL suspensions were centrifuged and used for UV-Vis characterization. Calibration based on the Lambert–Beer law was used to quantify the concentration of CBZ.

Total organic carbon (TOC) was measured using TOC-VCPN of Shimadzu Corporation of Japan. A combustion catalytic oxidation method of 680 °C is used. The measurement range is from 4 µg L^{-1} to 30 000 µg L^{-1}. The degradation intermediates were detected by mass spectrometry on Agilent HPLC-6500 Q-TOF in electrospray positive ion (ESI^+) mode with acetonitrile (solvent A) and ultrapure water with 0.1% V formic acid (solvent B) as mobile phase. A zorbax eclipse plus C18 column (1.8 µm, 2.1 × 50 mm) was used as separation column.

3. Results and discussion

3.1 Characterization of the photocatalysts

Fig. 1 shows the UV-Vis diffuse reflectance spectra of $BiVO_4$, $Pt/BiVO_4$, $MnO_x/BiVO_4$, $Co_3O_4/BiVO_4$, $Pt/BiVO_4/MnO_x$ and $Pt/BiVO_4/Co_3O_4$. The absorption edge of the prepared $BiVO_4$ is about 535 nm, demonstrating a strong absorption in the visible light region. No obvious shift of the absorption edge is observed when different cocatalysts were loaded on $BiVO_4$. The XRD patterns of the as-prepared $BiVO_4$, $Pt/BiVO_4/MnO_x$ and $Pt/BiVO_4/Co_3O_4$ are shown in Fig. 2. The diffraction peaks of all of the samples are identical to the peaks for the monoclinic scheelite phase of $BiVO_4$ (JCPDS 14-0688). The crystal structures of the co-loaded $BiVO_4$ show no changes compared with that of pure $BiVO_4$, implying that the
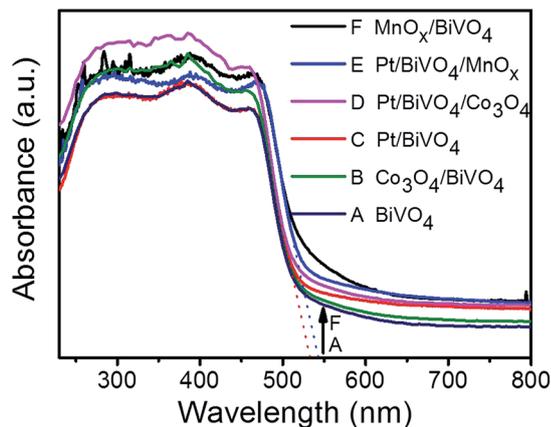
Fig. 1 UV-Vis DRS of different photocatalysts. The contents of the deposited Pt, MnO_x and Co_3O_4 are 0.2 wt%, 0.1 wt% and 0.1 wt%, respectively.
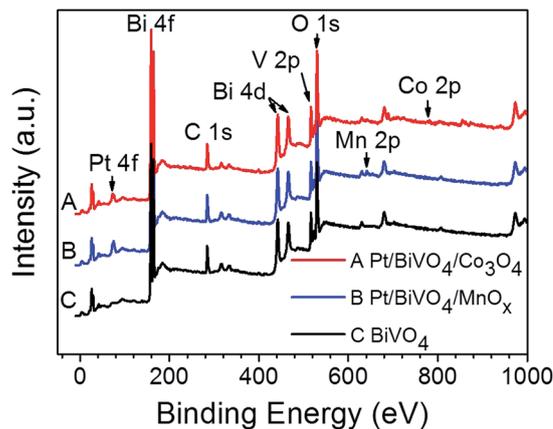

Fig. 3 XPS spectra of $BiVO_4$, $Pt/BiVO_4/Co_3O_4$ and $Pt/BiVO_4/MnO_x$. The contents of the deposited Pt is 0.2 wt%, Co_3O_4 and MnO_x are all 0.1 wt%.

cocatalysts are loaded onto the surface of the $BiVO_4$. N_2 adsorption–desorption isotherms (Fig. S1†) show that the co-loading of Pt and Co_3O_4 (MnO_x) did not change the framework of $BiVO_4$ and the BET surface areas of the three components photocatalysts $Pt/BiVO_4/Co_3O_4$ (MnO_x) are comparable with $BiVO_4$.

SEM images of $Pt/BiVO_4/Co_3O_4$ further demonstrate that the cocatalysts are deposited on the surface of the $BiVO_4$ (Fig. S2†). Furthermore, as reported by Li et al.,[26,27] the reduction cocatalyst Pt and oxidation cocatalyst Co_3O_4 may be deposited on the different facets of $BiVO_4$, which will facilitate the charge separation of electrons and holes.

The chemical states of the loaded cocatalysts were examined by XPS characterization. The Pt 4f peak located at binding energy of 70.7 eV was observed for both three components photocatalysts, indicating the existence of the metallic Pt (0) on $BiVO_4$ (Fig. 3). The Co 2p peaks at binding energies of 777.9 eV and 795.0 eV demonstrating that Co_3O_4 was

deposited on $BiVO_4$ (Fig. 4a).[26] The Mn 2p peaks are located at binding energies of 653.5 eV and 641.9 eV, which are between those of Mn_2O_3 and MnO_2 (Fig. 4b). Based on this, the deposited Mn species can be ascribed to MnO_x, where x is between 1.5 and 2.0.[27]
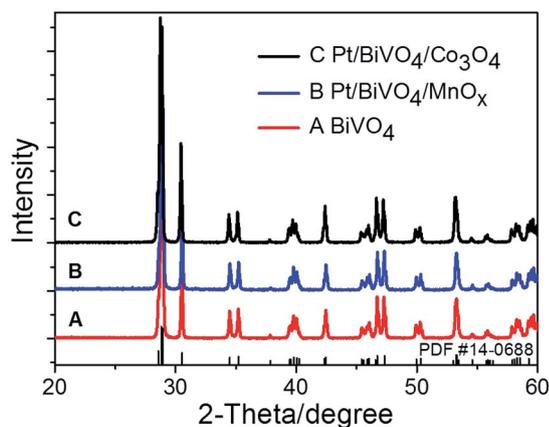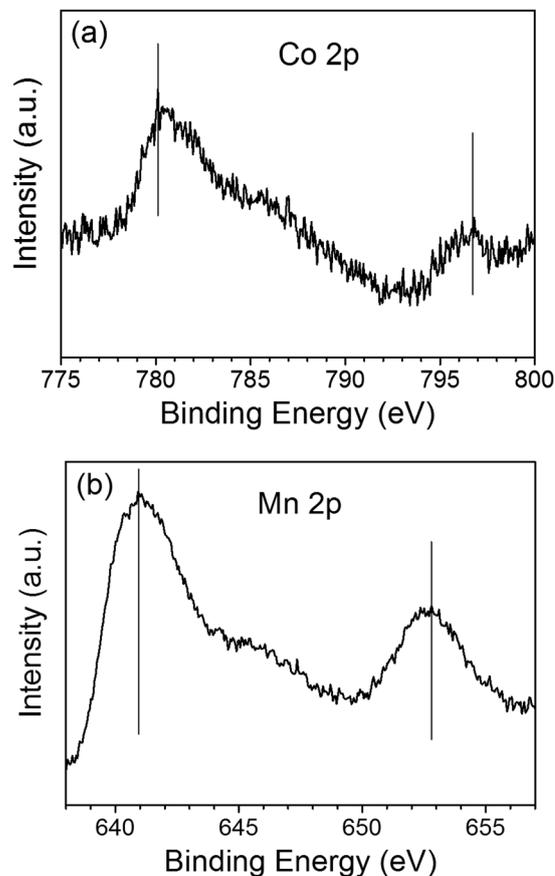

Fig. 4 The Co 2p XPS spectra of Co_3O_4 (a) and Mn 2p XPS spectra of MnO_x (b) deposited on $BiVO_4$. The contents of the deposited Co_3O_4 and MnO_x are all 0.1 wt%.

Fig. 2 XRD patterns of $BiVO_4$, $Pt/BiVO_4/MnO_x$ and $Pt/BiVO_4/Co_3O_4$. The contents of the deposited Pt is 0.2 wt%, Co_3O_4 and MnO_x are all 0.1 wt%.
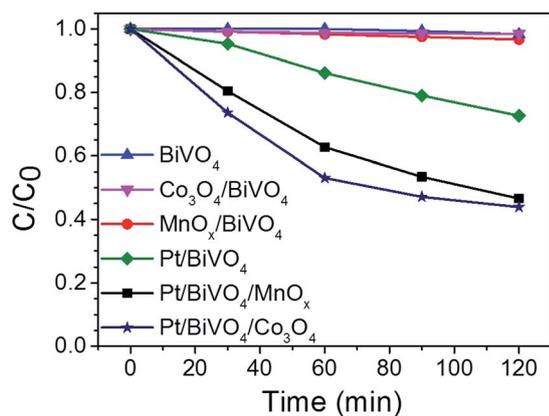
Fig. 5 Photocatalytic degradation of CBZ on different photocatalysts. Reaction conditions: 100 mL CBZ solution with initial concentration of 10 mg L^{-1}, catalyst dosage 1 g L^{-1}, the contents of the deposited Pt is 0.2 wt%, Co_3O_4 and MnO_x are all 0.1 wt% and 300 W Xe lamp ($\lambda > 420$ nm), top irradiation.
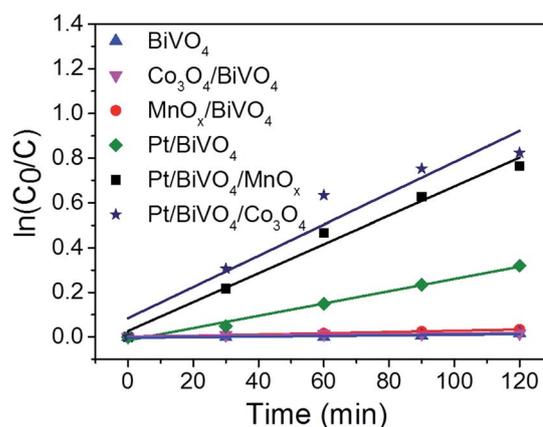

Fig. 6 Kinetic fitting of the CBZ degradation on different photocatalysts. Reaction conditions: 100 mL CBZ solution with initial concentration of 10 mg L^{-1}, catalyst dosage 1 g L^{-1}, the contents of the deposited Pt is 0.2 wt%, Co_3O_4 and MnO_x are all 0.1 wt% and 300 W Xe lamp ($\lambda > 420$ nm), top irradiation.

3.2 The effect of cocatalyst on photocatalytic degradation of carbamazepine

Fig. 5 shows the kinetic data of the photocatalytic degradation of CBZ on different photocatalysts. $BiVO_4$ without loaded cocatalyst exhibited a low removal (*ca.* 2%) in 120 min, and the removal was slightly enhanced when the oxidation cocatalyst MnO_x or Co_3O_4 was loaded on $BiVO_4$. When reduction cocatalyst Pt was deposited on $BiVO_4$, the removal of CBZ was enhanced to about 28% in 120 min. However, when Pt and Co_3O_4 were co-loaded on $BiVO_4$, the removal was significantly improved to *ca.* 56%, much higher than those of Pt/$BiVO_4$ and Co_3O_4/$BiVO_4$. Same trend was also observed when Pt and MnO_x were co-loaded on $BiVO_4$, yielding a removal of *ca.* 53% in 120 min, which is much higher than those of Pt/$BiVO_4$ and MnO_x/$BiVO_4$.

TOC analysis was carried out to evaluate the mineralization extent of CBZ on $BiVO_4$ and Pt/$BiVO_4$/Co_3O_4 photocatalysts (Fig. S3†). As shown in Fig. S3,† the TOC removal of CBZ in the presence of Pt/$BiVO_4$/Co_3O_4 is also much higher than that of $BiVO_4$. Long-term circulation measurement was carried out to check the stability of the photocatalyst Pt/$BiVO_4$/Co_3O_4. As shown in Fig. S4,† the photocatalytic activity of Pt/$BiVO_4$/Co_3O_4 can be well maintained even after three runs, only less than 5% decreasing, indicating the excellent stability and durability of the three components photocatalyst.

The plots of $\ln(C_0/C)$ *versus* the reaction time (t) is presented in Fig. 6. All of the fitted curves show high corresponding apparent coefficients, revealing that the photocatalytic degradation of CBZ over different photocatalysts is in line with pseudo-first-order kinetic. The values of the rate constant k for different photocatalysts are listed in Table 1. The single loading of either oxidation cocatalyst (entry 2 and 3) or reduction cocatalyst (entry 4) can somewhat enhance the activity of $BiVO_4$, demonstrating the roles of cocatalysts played in the facilitating of charge transfer of photogenerated holes or electrons; however, the

enhancement is limited. The promotion caused by the reduction cocatalyst loading is more obvious than the oxidation cocatalyst loading, indicating that the reduction half-reaction may be the rate-determining step.[26] When reduction and oxidation cocatalysts were co-loaded on $BiVO_4$, the rate constants (entry 5 and 6) were significantly improved. The k for Pt/$BiVO_4$/MnO_x is 23 times of MnO_x/$BiVO_4$ and 2.3 times of Pt/$BiVO_4$. Similarly, the k for Pt/$BiVO_4$/Co_3O_4 is 54 times of Co_3O_4/$BiVO_4$ and 2.5 times of Pt/$BiVO_4$. Both of the three components photocatalysts show obvious synergetic effect of the dual cocatalysts ($k_5 > k_3 + k_4$, $k_6 > k_2 + k_4$). This demonstrates that only when the reduction and oxidation reactions were accelerated simultaneously we can get the much higher reaction rate than any other one.

The roles of cocatalysts played in facilitating photogenerated charges transfer can be further demonstrated by the photoelectrochemical measurements. As shown in Fig. S5,† the photocurrent density of the three components photocatalysts Pt/$BiVO_4$/Co_3O_4 and Pt/$BiVO_4$/MnO_x are higher

Table 1 Apparent first-order rate constant k for degradation of CBZ over different photocatalysts

Entry	Photocatalysts	k^a ($\times 10^{-3}$ min^{-1})
1	$BiVO_4$	0.12
2	Co_3O_4/$BiVO_4$	0.13
3	MnO_x/$BiVO_4$	0.28
4	Pt/$BiVO_4$	2.75
5	Pt/$BiVO_4$/MnO_x	6.46
6	Pt/$BiVO_4$/Co_3O_4	6.98

^{a} The apparent first-order rate constant k is calculated from the equation: $\ln(C_0/C) = kt$, where C_0 is the initial concentration and C is the concentration at certain time t. Reaction conditions: 100 mL CBZ solution with initial concentration of 10 mg L^{-1}, catalyst dosage 1 g L^{-1}, the contents of the deposited Pt is 0.2 wt%, Co_3O_4 and MnO_x are all 0.1 wt% and 300 W Xe lamp ($\lambda > 420$ nm), top irradiation.
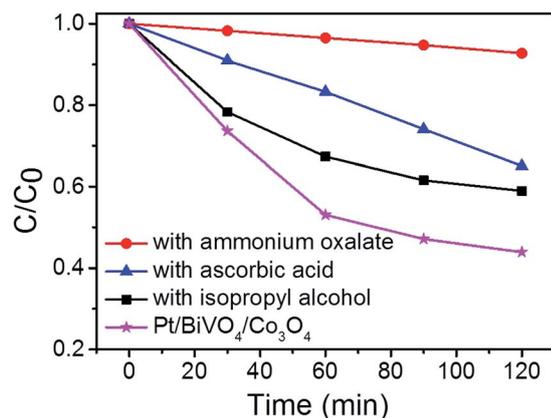
Fig. 7 Effect of scavengers on photocatalytic degradation of CBZ over Pt/BiVO$_4$/Co$_3$O$_4$ photocatalyst. Reaction conditions: 100 mL CBZ solution with initial concentration of 10 mg L^{-1}, scavenger concentration 50 mmol L^{-1}, catalyst dosage 1 g L^{-1}, the contents of the deposited Pt and Co$_3$O$_4$ are 0.2 wt% and 0.1 wt% respectively and 300 W Xe lamp (λ > 420 nm), top irradiation.
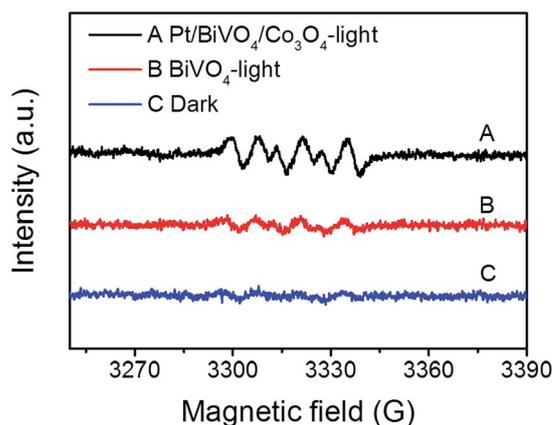

Fig. 8 *In situ* ESR spectra of DMPO-O$_2$$^{\bullet-}$ generated by BiVO$_4$ and Pt/BiVO$_4$/Co$_3$O$_4$ after 10 min of visible-light irradiation (λ > 420 nm). The signal obtained in the presence of photocatalyst but without light irradiation is denoted as "Dark".

than that of bare BiVO$_4$. This demonstrating that due to the co-loading of cocatalysts, the photo-generated charges can be more efficiently trapped, which makes more photo-generated holes survived on the three components photocatalysts. Moreover, the photocurrent of Pt/BiVO$_4$/Co$_3$O$_4$ is higher than Pt/BiVO$_4$/MnO$_x$, demonstrating that the photogenerated holes (h$^+$) would transfer easier from BiVO$_4$ to Co$_3$O$_4$ than to MnO$_x$, which cause the superior performance of Pt/BiVO$_4$/Co$_3$O$_4$ than Pt/BiVO$_4$/MnO$_x$ on the photocatalytic CBZ degradation. The electrochemical impedance spectra (EIS) of BiVO$_4$ and Pt/BiVO$_4$/Co$_3$O$_4$ further demonstrate the role of cocatalysts played in facilitating photo-generated charges transfer. As shown in Fig. S6,† the arc radius on the EIS plot of Pt/BiVO$_4$/Co$_3$O$_4$ is smaller than that of BiVO$_4$, implying that the co-loading of Pt and Co$_3$O$_4$ make photo-generated charges transfer easier.

3.3 Identification of main reactive species

To identify the main reactive species in the photocatalytic degradation process, trapping experiments were conducted on Pt/BiVO$_4$/Co$_3$O$_4$ photocatalyst and the results are shown in Fig. 7. The addition of ammonium oxalate (AO, scavengers of h$^+$ radical) has significant inhibition on CBZ degradation, indicating that h$^+$ is crucial active species. The addition of ascorbic acid (VC, scavengers of $\cdot$O$_2$$^-$ radical) and isopropyl alcohol (IPA, scavengers of $\cdot$OH radical) have feeble inhibition, which reveals that $\cdot$O$_2$$^-$ and $\cdot$OH serve as synergistic active species but not as the most crucial active species. Similar results were observed for Pt/BiVO$_4$/MnO$_x$ photocatalyst (Fig. S7†).

In order to gain direct evidence for the reactive radicals involved in the photocatalytic process, ESR analysis was employed using DMPO as trapping agent. As shown in Fig. 8, the sextet ESR signal centered at g = 2.0065 can be assigned to DMPO-O$_2$$^{\bullet-}$. These results provide evidence of $\cdot$O$_2$$^-$ formed in the presence of the photocatalyst BiVO$_4$ and Pt/BiVO$_4$/Co$_3$O$_4$.

Moreover, the signal of $\cdot$O$_2$$^-$ generated after 10 min of illumination on Pt/BiVO$_4$/Co$_3$O$_4$ is more obvious than those for BiVO$_4$, demonstrating the roles of cocatalysts played in facilitating charge separation and transfer.

3.4 Degradation pathway of CBZ photocatalyzed by Pt/BiVO$_4$/Co$_3$O$_4$

Based on the LC-ESI-MS results (Table S1 and Fig. S8†), the possible degradation pathway of CBZ photocatalyzed by Pt/BiVO$_4$/Co$_3$O$_4$ was proposed in Fig. 9. First of all, alkene double bond of CBZ was attack by $\cdot$OH radical and transferred into intermediate **P6** and **P9**.[33–35] Intermediate **P6** was further hydroxylated to generate **P2** which might be further oxidized to generate **P8**.[35] As for intermediate **P9**, it might be further oxidized by $\cdot$O$_2$$^-$ and photo-generated h$^+$ to convert into **P4** and **P7**.[34] After aldehyde oxidation reaction in **P4**, **P5** was generated and further transferred to **P8**.[35] Product **P7** might undergo several successive steps including deamination and decarboxylation to produce **P1** and **P3**.[7,34,36] Further oxidized by $\cdot$OH, h$^+$ and $\cdot$O$_2$$^-$, **P3** and **P8** could be finally mineralized into CO$_2$ and H$_2$O *via* ring–rupturing reaction.

The proposed mechanism of photocatalytic degradation of CBZ on Pt/BiVO$_4$/Co$_3$O$_4$ (MnO$_x$) is shown in Fig. 10. Under visible light irradiation, photo-generated electrons would transfer from the conduction band (CB) of BiVO$_4$ to the reduction cocatalyst Pt, on which the adsorbed O$_2$ is reduced to $\cdot$O$_2$$^-$ radical. Meanwhile, the holes would migrate from the valence band (VB) of BiVO$_4$ to the oxidation cocatalyst Co$_3$O$_4$ (MnO$_x$), where the adsorbed CBZ or H$_2$O are oxidized to CO$_2$ and $\cdot$OH respectively. The produced $\cdot$O$_2$$^-$ and $\cdot$OH also participate in the degradation of CBZ, which is consistent with the trapping experiment results. The co-loading of both the reduction cocatalyst Pt and oxidation cocatalyst Co$_3$O$_4$ (MnO$_x$) is beneficial for the efficient separation and transfer of the photo-generated electrons and holes, accounts for the high photocatalytic activity of CBZ degradation.
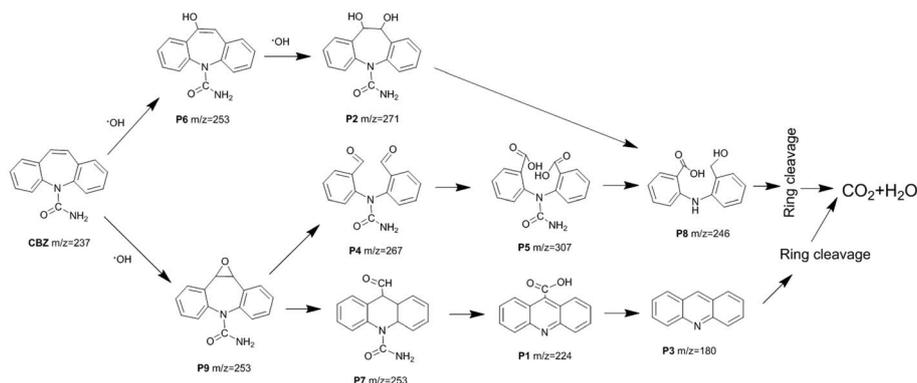
Fig. 9 Proposed degradation pathway of CBZ by Pt/BiVO₄/Co₃O₄ photocatalyst.
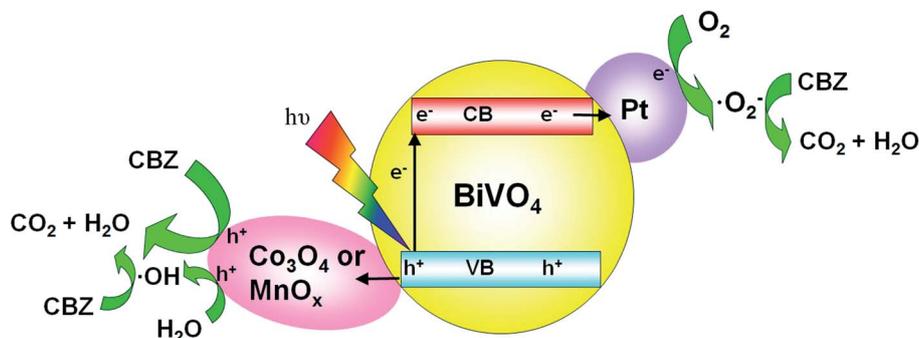

Fig. 10 Schematic description of the mechanism for the photocatalytic degradation of CBZ on Pt/BiVO₄/Co₃O₄ (MnOₓ) photocatalyst under visible light irradiation.

4. Conclusion

A synergetic effect in photocatalytic degradation of CBZ was achieved when reduction cocatalyst Pt and oxidation cocatalyst Co₃O₄ (MnOₓ) were co-loaded on BiVO₄. The co-loading of both the reduction cocatalyst and oxidation cocatalyst can facilitate the separation and transfer of the photo-generated electrons and holes, which is responsible for the high photocatalytic activity of the three components photocatalysts. This work further demonstrates the universality of the strategy of dual-cocatalysts, which would be useful to construct highly efficient photocatalyst for pharmaceuticals degradation.

Conflicts of interest

The authors declare no competing financial interest.

Acknowledgements

References

1 J. Rivera-Utrilla, M. Sanchez-Polo, M. A. Ferro-Garcia, G. Prados-Joya and R. Ocampo-Perez, *Chemosphere*, 2013, **93**, 1268–1287.
2 Y. J. Zhang, S. U. Geissen and C. Gal, *Chemosphere*, 2008, **73**, 1151–1161.
3 T. Heberer, *Toxicol. Lett.*, 2002, **131**, 5–17.
4 K. Fent, A. A. Weston and D. Caminada, *Aquat. Toxicol.*, 2006, **76**, 122–159.
5 P. A. K. Reddy, P. V. L. Reddy, E. Kwon, K. H. Kim, T. Akter and S. Kalagara, *Environ. Int.*, 2016, **91**, 94–103.
6 S. Murgolo, V. Yargeau, R. Gerbasi, F. Visentin, N. El Habra, G. Ricco, I. Lacchetti, M. Carere, M. L. Curri and G. Mascolo, *Chem. Eng. J.*, 2017, **318**, 103–111.
7 M. Nawaz, W. Miran, J. Jang and D. S. Lee, *Appl. Catal., B*, 2017, **203**, 85–95.
8 A. Carabin, P. Drogui and D. Robert, *J. Taiwan Inst. Chem. Eng.*, 2015, **54**, 109–117.
9 A. Y. C. Tong, R. Braund, D. S. Warren and B. M. Peake, *Cent. Eur. J. Chem.*, 2012, **10**, 989–1027.

10 A. Cincinelli, T. Martellini, E. Coppini, D. Fibbi and A. Katsoyiannis, *J. Nanosci. Nanotechnol.*, 2015, **15**, 3333–3347.

11 D. Kanakaraju, B. D. Glass and M. Oelgemoller, *Environ. Chem. Lett.*, 2014, **12**, 27–47.

12 Y. X. Gao, G. Yu, K. Liu, S. B. Deng, B. Wang, J. Huang and Y. J. Wang, *Chem. Eng. J.*, 2017, **330**, 157–165.

13 X. Chen, W. Y. Lu, T. F. Xu, N. Li, Z. X. Zhu, G. Q. Wang and W. X. Chen, *Chem. Eng. J.*, 2017, **328**, 853–861.

14 L. Lin, H. Y. Wang and P. Xu, *Chem. Eng. J.*, 2017, **310**, 389–398.

15 L. Lin, H. Y. Wang, W. B. Jiang, A. R. Mkaouar and P. Xu, *J. Hazard. Mater.*, 2017, **333**, 162–168.

16 Y. B. Ding, G. L. Zhang, X. R. Wang, L. H. Zhu and H. Q. Tang, *Appl. Catal., B*, 2017, **202**, 528–538.

17 J. H. Yang, D. G. Wang, H. X. Han and C. Li, *Acc. Chem. Res.*, 2013, **46**, 1900–1909.

18 F. Y. Wen and C. Li, *Acc. Chem. Res.*, 2013, **46**, 2355–2364.

19 K. Wenderich and G. Mul, *Chem. Rev.*, 2016, **116**, 14587–14619.

20 T. D. Nguyen, Q. T. P. Bui, T. B. Le, T. M. Altahtamouni, K. B. Vu, D. V. N. Vo, N. T. H. Le, T. D. Luu, S. S. Hong and K. T. Lim, *RSC Adv.*, 2019, **9**, 23526–23534.

21 D. Gao, W. Liu, Y. Xu, P. Wang, J. Fan and H. Yu, *Appl. Catal., B*, 2020, **260**, 118190.

22 S. C. Sun, Y. C. Zhang, G. Q. Shen, Y. T. Wang, X. L. Liu, Z. W. Duan, L. Pan, X. W. Zhang and J. J. Zou, *Appl. Catal., B*, 2019, **243**, 253–261.

23 H. G. Yu, R. R. Yuan, D. D. Gao, Y. Xu and J. G. Yu, *Chem. Eng. J.*, 2019, **375**, 121934.

24 M. H. Ai, J. W. Zhang, R. J. Gao, L. Pan, X. W. Zhang and J. J. Zou, *Appl. Catal., B*, 2019, **256**, 117805.

25 R. G. Li, X. P. Tao, R. T. Chen, F. T. Fan and C. Li, *Chem.–Eur. J.*, 2015, **21**, 14337–14341.

26 R. G. Li, H. X. Han, F. X. Zhang, D. G. Wang and C. Li, *Energy Environ. Sci.*, 2014, **7**, 1369–1376.

27 R. G. Li, F. X. Zhang, D. G. Wang, J. X. Yang, M. R. Li, J. Zhu, X. Zhou, H. X. Han and C. Li, *Nat. Commun.*, 2013, **4**, 7.

28 F. Lin, Y. N. Zhang, L. Wang, Y. L. Zhang, D. G. Wang, M. Yang, J. H. Yang, B. Y. Zhang, Z. X. Jiang and C. Li, *Appl. Catal., B*, 2012, **127**, 363–370.

29 B. J. Ma, F. Y. Wen, H. F. Jiang, J. H. Yang, P. L. Ying and C. Li, *Catal. Lett.*, 2010, **134**, 78–86.

30 L. C. Mu, Y. Zhao, A. L. Li, S. Y. Wang, Z. L. Wang, J. X. Yang, Y. Wang, T. F. Liu, R. T. Chen, J. Zhu, F. T. Fan, R. G. Li and C. Li, *Energy Environ. Sci.*, 2016, **9**, 2463–2469.

31 F. Lin, D. Wang, Z. Jiang, Y. Ma, J. Li, R. Li and C. Li, *Energy Environ. Sci.*, 2012, **5**, 6400–6406.

32 D. E. Wang, R. G. Li, J. Zhu, J. Y. Shi, J. F. Han, X. Zong and C. Li, *J. Phys. Chem. C*, 2012, **116**, 5082–5089.

33 X. Y. Gao, X. C. Zhang, Y. W. Wang, S. Q. Peng, B. Yue and C. M. Fan, *Chem. Eng. J.*, 2015, **273**, 156–165.

34 Y. Guo, P. F. Wang, J. Qian, Y. H. Ao, C. Wang and J. Hou, *Appl. Catal., B*, 2018, **234**, 90–99.

35 J. Cao, W. S. Nie, L. Huang, Y. B. Ding, K. L. Lv and H. Q. Tang, *Appl. Catal., B*, 2019, **241**, 18–27.

36 J. Xu, L. Li, C. S. Guo, Y. Zhang and W. Meng, *Appl. Catal., B*, 2013, **130**, 285–292.